

# Capturing Important Statistics of a Fading/Shadowing Channel for Network Performance Analysis

Young Yong Kim and San-qi Li, *Member, IEEE*

**Abstract**— In this paper we identify important characteristics of a fading/shadowing channel and present the work of measurement-based channel modeling for packet-level network queueing analysis. Our integration of wireless channel modeling and data queueing analysis at the packet-level provides a unique approach to study the effect of various channel dynamics on high-layer network performance, which otherwise cannot be captured through the traditional bit-level physical-layer channel modeling. In our study, the channel statistics are decomposed into three frequency regions [i.e., low (LF), mid (MF), and high (HF)]; the statistics in each frequency region is found to have significantly different impact on the queueing performance. While the HF statistics can be largely ignored in channel modeling due to their negligible impact on queueing performance, the LF statistics play the most important role in channel modeling because of substantial impact on queueing performance. Since the shadowing mainly represents the LF behavior of a channel, its dynamics are found to have a dominant effect on network performance as compared to the effect of multipath fading dynamics. In wireless networks, there are many other system factors which may change the channel dynamics, such as mobile user driving patterns, and forward-error-correction (FEC) coding (fixed or adaptive) using automated repeat request (ARQ) scheme. Our study further examines the individual impact of these factors on the network performance. In the measurement-based channel modeling, we use a Markov chain modeling technique to match the important channel statistics for queueing system analysis. The study shows an excellent agreement in queueing solutions between using the real original channel traces and using the sequences generated by the matched Markov chain models.

**Index Terms**— Channel modeling, multimedia communication, multipath fading, queueing analysis.

## I. INTRODUCTION

**E**ARLY WORK in wireless channel modeling focused on the stochastic modeling of channel dynamics at physical layer, measured by received signal strength or bit error rate (BER) [1]–[6]. Such physical-layer models cannot be directly used to evaluate high layer network performance, such as packet queueing delay and loss. For instance, a few bit errors within a packet, which is the basic data unit at the wireless *link layer*, will cause the entire loss of the packet. Further, a single

packet loss within a message, which can be the basic data unit at the end-to-end *network layer*, will cause the entire loss of the message as defined by many network control protocols. It is therefore imperative to develop sophisticated packet-level wireless channel models, which can be used by network engineers to simulate and analyze the high-layer performance in wireless network protocol development. Limited work is available on packet-level wireless modeling [7]–[10]. One commonly adopted method is to use two-state Markov chain to match the average ON (success) and OFF (loss) periods of packet transmission measured on a multipath fading channel [8]. Note that it is unlikely to develop a generic stochastic model for capturing the great diversity of wireless channel dynamics, which are time-varying, frequency-selective, and highly dependent on many other system factors such as noise, distance, mobile speed, multipath interference, power control, coding, etc. In other words, a successful modeling technique must be measurement based to capture real channel statistics under various conditions. To make this modeling feasible, our first objective is to identify what are the important statistics of fading channel to packet-level network performance. In this paper, shadowing is defined as the signal attenuation by irregular terrains, which occurs over large area and large time scale, and multipath fading is defined as the signal attenuation by moving receiver such as Rayleigh and Rician fading. Our recent study of multipath Rayleigh fading channel dynamics [11] indicates that the queueing performance can be strongly affected by the second-order statistics of multipath fading in low-frequency (LF) region. Further, the queueing performance is largely dependent on the interaction between channel power spectrum and data arrival power spectrum, whichever has more LF power will have dominant impact on the queueing performance. Note that the data arrival power spectrum provides the measure of data arrival correlation behavior. In this paper, we investigate the impact of multipath and shadowing fading channel dynamics on the packet-level data queueing performance.

The channel dynamics at the packet level is represented by a data packet service rate process  $R_c(t)$ , which in general can be considered as a stationary random process. For simplicity,  $R_c(t)$  is also referred to as the channel process. It is difficult to obtain an exact description of  $R_c(t)$  and only its statistics are measurable. The first-order statistics are described by the steady state probability density function or cumulative distribution function (CDF). The second-order statistics are specified by the autocorrelation function or power spectral density function (PSD). Comparatively, higher order statistics

Manuscript received December 1, 1997; revised July 1998. This work was supported by National Science Foundation under Grant NCR-9314387, Southwestern Bell, and Intel Technology for Education 2000 equipment grant.

Y. Y. Kim was with the Department of Electrical and Computer Engineering, University of Texas at Austin, Austin, TX 78712 USA. He is now with the Wireless Network Management Research Group, Telcordia Technologies, Red Bank, NJ 07701-5699 USA (e-mail: ykim@telcordia.com).

S. Li is with the Department of Electrical and Computer Engineering, University of Texas at Austin, Austin, TX 78712 USA (e-mail: sanqi@lobe.ece.utexas.edu).

Publisher Item Identifier S 0733-8716(99)03078-4.

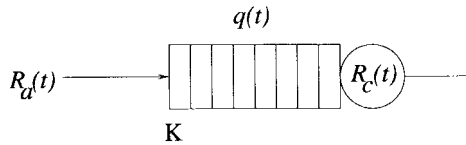


Fig. 1. Wireless multimedia queuing system.

as characterized by bispectrum and trispectrum are more difficult to measure. Let us consider a queueing process with finite buffer capacity as shown in Fig. 1, whose service process is  $R_c(t)$  and buffer capacity  $K$  is measured in packet units. The data arrival process  $R_a(t)$  is also a random rate process, which may represent a multimedia traffic stream with its own measured statistical properties. Using the fluid flow assumption, one can describe the queueing process by

$$q(t + \Delta) = \max[0, q(t) + R_a(t) - R_c(t)] \quad (1)$$

where  $q(t)$  is the queue length at time  $t$  subject to  $q(t + \Delta) \leq K$ . Given the channel transmission capacity  $\mu$  measured in packet units at  $\Delta$  time interval and the error probability per packet at time  $t$  denoted by  $\text{PER}(t)$ , we define

$$R_c(t) = [1 - \text{PER}(t)]\mu. \quad (2)$$

Hence, the  $R_c(t)$  statistics are simply a shifted, normalized version of the PER statistics. The average channel capacity is given by  $\{1 - E[\text{PER}(t)]\}\mu$ . Similarly,  $R_a(t)$  may represent the number of packet arrivals at the time interval  $[t, t + \Delta)$ .

Most queueing analyses of multimedia traffic so far have focused on wireline networks such as ATM, where the service rate is assumed to be constant. Under the assumption of a constant service rate, the studies in [13]–[15] indicate that only the first- and second-order statistics of the arrival process are important to steady-state queue length and loss rate solutions, whereas its higher order statistics can be neglected, given a properly selected frequency range for the measurement. Most importantly, the queueing performance is mainly governed by LF behavior of the arrival process. That is, higher energy of the arrival process in LF bands means requirement of more buffer capacity and/or larger link bandwidth for packet transmission. In real networks, most multimedia traffic streams exhibit high energy located in LF bands, which is equally described by large time-varying scale, high correlation, or long range dependence.

Intuitively, one may characterize a queueing system by a nonlinear low pass filter, where the HF variation of the input traffic can be well absorbed into the buffering but its LF variation remains largely unchanged [16], [17]. For instance, the lowest frequency component of the traffic, i.e., the DC term, is its average arrival rate, which always stays intact through a queueing system unless with traffic loss by buffer blocking. Moreover, such low-frequency behavior of the traffic will remain largely unchanged through a network of interconnected queues [18].

The queueing analysis in wireline networks can be extended to wireless. Essentially, the effect of the service rate statistics is the same as the effect of the arrival rate statistics on the queueing process. For instance, if we define  $R'_c(t) = \mu - R_c(t)$

where  $\mu$  is the maximum of  $R_c(t)$ , the queueing process can be described by

$$q(t + \Delta) = \max[0, q(t) + R_a(t) + R'_c(t) - \mu]. \quad (3)$$

It is obvious that  $R'_c(t)$  plays the same role as  $R_a(t)$  in the queueing process. The statistics of  $R'_c(t)$  are just a “shifted” version of the original  $R_c(t)$  statistics. Therefore, only the first- and second-order statistics of the fading channel need to be measured and captured, especially in the LF band. The queueing performance depends on the interplay between channel and arrival statistics. If the arrival process contains much more LF energy than the channel process, one may completely ignore the channel statistics in modeling because the queueing performance is governed by the arrival statistics, and vice versa. Our study then focuses on the comparison of channel PSD and arrival PSD in LF band under various circumstances. Once the channel is identified to contain significant LF energy as compared to the arrival process, both first and second-order statistics in LF are important for the channel modeling in queueing analysis.

In [14], the input traffic characteristics is decomposed into three frequency regions (LF, MF, and HF) and the traffic statistics in each individual region is found to have significantly different impact on buffer capacity and transmission bandwidth requirement. Based on the same principle, one can divide channel dynamics into the three frequency regions and similarly examine the impact of the shadowing and multipath fading. It is obvious that the queueing performance depends on the combination effect of arrival and channel statistics. Our study indicates that the LF and MF arrival/channel statistics are most important to capture in modeling due to their substantial impact on the queueing performance. In contrast, the HF arrival/channel statistics can be largely ignored because of their negligible impact on queueing performance. Since the shadowing mainly represents the low-frequency behavior of a channel, its dynamics are found to have dominant effect on network performance as compared to the effect of multipath fading dynamics. Moreover, the shadowing fading dynamics are strongly dependent on many other system factors, such as mobile user driving patterns and forward-error-correction (FEC) coding (fixed or adaptive) using automated repeat request (ARQ) scheme. Our study further examines the individual impact of these factors on the network performance. The fading channel statistics in the downtown Austin area is used as an example of a typical large scale fading scenario in this paper.

Similar to the modeling of the arrival process, one can use a measurement-based modeling technique [13], called SMAQ, to build a Markov modulated process (MMP) to match the measured first- and second-order channel statistics. An MMP process is defined by both rate vector  $\vec{\gamma}$  and Markov chain transition rate matrix  $\mathbf{Q}$ . While  $\vec{\gamma}$  defines the service rate [or, arrival rate in case of  $R_a(t)$ ] in each state,  $\mathbf{Q}$  characterizes the time dynamics of the rate process. For  $R_c(t)$  modeling, the service rate is assumed to be exponential in each state. For  $R_a(t)$  modeling, the arrival rate is assumed to be Poisson in each state. Since both  $R_c(t)$  and  $R_a(t)$  are independently modeled by MMP, the queueing system is formulated as a

finite quasi-birth-death process, which can be numerically analyzed by the Folding algorithm [19]. Note that MMP has been commonly adopted for service and arrival process modeling in queueing fields.

One may further decompose the arrival process into a number of independent data sources. Since the emphasis of this paper is placed on the channel modeling, we simply assume that each data source is modeled by an i.i.d. two-state MMP, alternating between ON and OFF periods. Each exponential ON period represents the generation of a single message consisting of multiple packets. While in ON period, packets are generated at a Poisson rate. Each OFF period represents the inactive time interval between two adjacent message generations. Note that the superposition of independent MMP's is still an MMP. As one will see, our queueing solutions based on the modeling match well with the simulation results using the original wireless channel trace.

The remainder of the paper is organized as follows. Section II explains our measurement-based channel modeling framework. Section III investigates the queue response to various fading channel dynamics, using both computer simulation and analytical modeling techniques. Section IV is the conclusion.

## II. CHANNEL AND ARRIVAL STATISTICS

### A. Channel Statistics at Signal-Strength Level

Channel fading behavior can be classified into shadowing dynamics and multipath fading dynamics [20]. The shadowing dynamics describes the signal attenuation due to the motion of a mobile station over a large irregular terrain. The multipath fading dynamics captures the signal attenuation by multiple versions of transmitted signals arrived at a receiver with small changes in position. In general wireless communication environments, both shadowing and multipath fading, manifest themselves simultaneously where shadowing defines average path loss at a certain position with log-normal deviation from the mean, and multipath fading introduces further fast variation of received signal strength [20]. Let  $h(t)$  be the impulse response of a fading channel. One can then decompose the magnitude of  $h(t)$  into two parts

$$|h(t)| = \alpha_s(t) \times \alpha_f(t) \quad (4)$$

where  $\alpha_s(t)$  and  $\alpha_f(t)$  are the attenuation of shadowing and multipath fading, respectively.

Because of the highly variable wireless fading environment, any realistic channel modeling must be measurement-based. As an illustrative example, our study is based on the real fading statistics collected in the downtown area of Austin City at 1.9 GHz with continuous wave (CW) [21]. Fig. 2 shows a simplified map of the measurement coverage in the downtown Austin area. The base station is located at Congress and 7th Street. The car was driven at normal speed on every street in the map to collect the CW attenuation at 1 ms interval. The size of area covered by the measurement is approximately 400 m in diameter.

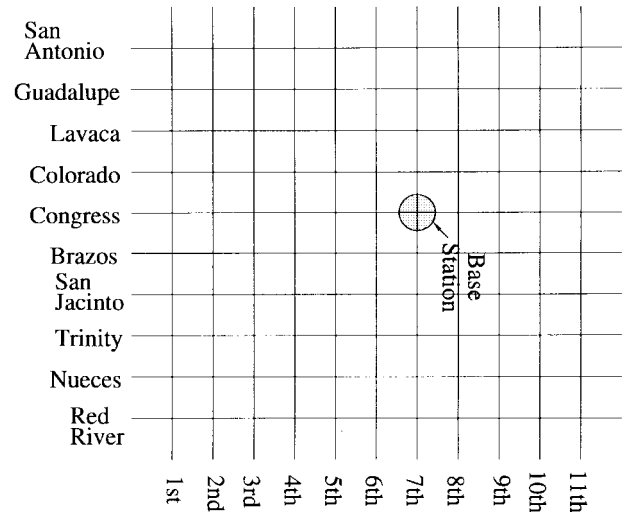


Fig. 2. A simplified map of downtown Austin area.

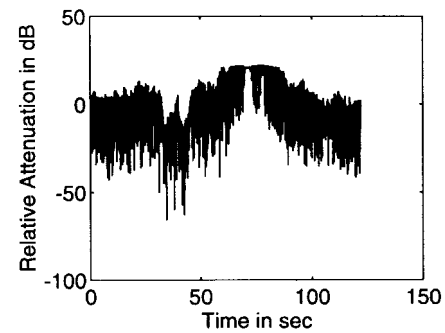


Fig. 3. Measured signal attenuation in downtown Austin area.

Fig. 3 shows an example of short segment of time series of attenuation in the downtown Austin area. This segment represents a drive along one street (Trinity). The attenuation in Fig. 3 are relative values and do not represent the actual received signal strength. Both shadowing and multipath fading are included in the measurement.

### B. Channel Statistics at Packet Level

One can use the collective fading profile at signal-strength level to generate various kinds of time series of packet error rate,  $PER(t)$ , given the system conditions such as modulation method, packet size, and error correction coding schemes. The statistics of  $PER(t)$  provides the probabilistic description of the packet loss process.

Denote the average bit energy of the received signal by  $E_b$  and the noise power density by  $N_0$ , within a cell. Assuming  $|h(t)|$  is normalized, the received bit-energy-to-noise-ratio time series is then represented by

$$SNR(t) = |h(t)|^2 E_b / N_0. \quad (5)$$

Based on a given channel modulation scheme, one can convert the signal-to-noise ratio (SNR) time series to bit error rate time series (BER). In our study, we assume to use the ideal  $\pi/4$  QPSK modulation scheme, such that one can write [22]

$$BER(t) = Q\left(\sqrt{2SNR(t)}\right) \quad (6)$$

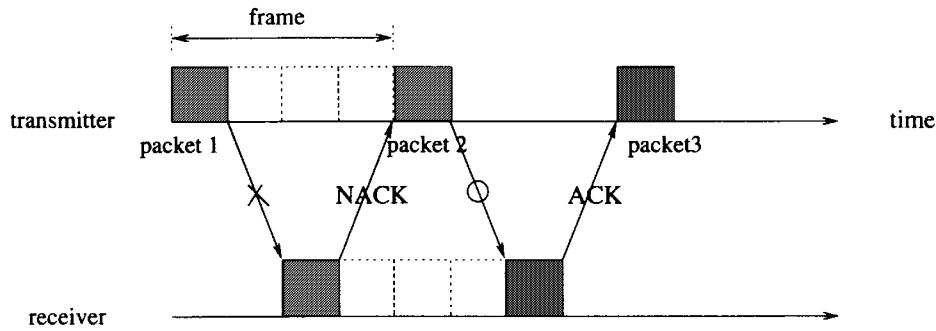


Fig. 4. Frame structure.

where  $Q(\cdot)$  is defined as

$$Q(z) = \frac{1}{\sqrt{2\pi}} \int_z^\infty e^{-x^2/2} dx. \quad (7)$$

The conversion from the BER time series to packet error rate time series (PER) is further dependent on its selected channel coding scheme. Without error correction coding

$$PER(t) = 1 - [1 - BER(t)]^n \quad (8)$$

where  $n$  is the number of bits in a packet, including error detection coding bits if any. If an error correction code is employed with capability of correcting up to  $m$  bit errors

$$PER(t) = \sum_{i=m+1}^n \binom{n}{i} BER(t)^i (1 - BER(t))^{n-i}. \quad (9)$$

One assumption made in (8) and (9) is that the fading time variation is slow as compared to the packet transmission time, such that  $BER(t)$  remains virtually unchanged during a packet transmission time. In other words, we take the average of the original  $SNR(t)$  in each adjacent packet transmission interval to generate the packet-level  $BER(t)$  trace. This assumption has been verified by comparison of the queueing solutions between the original bit-level BER trace and the averaged packet-level BER trace in [11]. It is also intuitively clear since the bit-level BER variation only contributes to the high frequency behavior of the channel statistics, which has negligible impact on the queueing solutions as one will see in Section III-B.

$PER(t)$  gives the probability of packet loss at time  $t$  on the channel. Assume to use a time division multiplexing access scheme on the wireless network, where each time frame is divided into a fixed number of slots and each slot represents a channel to transmit one packet per frame. Using the frequency division duplex (FDD) scheme, both upstream and downstream links will have a different frequency bandwidth. Here we only consider the data queueing process associated with a single channel. A packet will stay in the queue at the transmitter until it is successfully received and acknowledged by the receiver.

According to the standard stop-and-wait ARQ flow control scheme, a new packet will not be sent out until the previous packet has been successfully acknowledged by the receiver. Since the packet propagation time in a typical wireless environment is substantially shorter than the frame size, it is reasonable to assume that, before the next time slot becomes available, the transmitter will know if the packet transmission

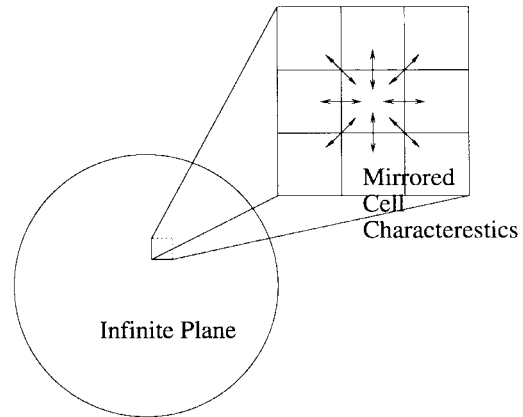


Fig. 5. Infinite mirrored cell model.

in the current slot is successful, as described in Fig. 4. In other words, the same packet will be retransmitted in the next time slot if it fails in the current slot with the probability  $PER(t)$ . In our study, we assume four time slots per frame as in Fig. 4. We further adopt the *type I* ARQ scheme [23] where both FEC coding and ARQ control scheme are used to achieve better throughput and more reliable communication.

The data packet service rate process is therefore defined by

$$R_c(t) = [1 - PER(t)]\mu \quad (10)$$

where  $\mu^{-1}$  is the frame interval, since there is one packet transmission on each channel per frame. The  $R_c(t)$  statistics is just a shifted, normalized version of the PER statistics. The average channel capacity is given by

$$E[R_c(t)] = \{1 - E[PER(t)]\}\mu. \quad (11)$$

### C. Channel Statistic Measurement

To use the fading sequence collected over a single cell for generic network analysis, we further assume an imaginary infinite size cellular system where all cells have same dimension, size, and attenuation characteristics as our measurement area in downtown Austin. Fig. 5 depicts the concept of our imaginary cellular system. Note that adjacent cells have the same attenuation characteristics which are mirrored images of each other with respect to the cell boundaries. On this imaginary cellular system, we consider two driving patterns: directional versus random. Each time when a mobile user is at a cross section of the street, it turns left with probability  $P_l$ ,

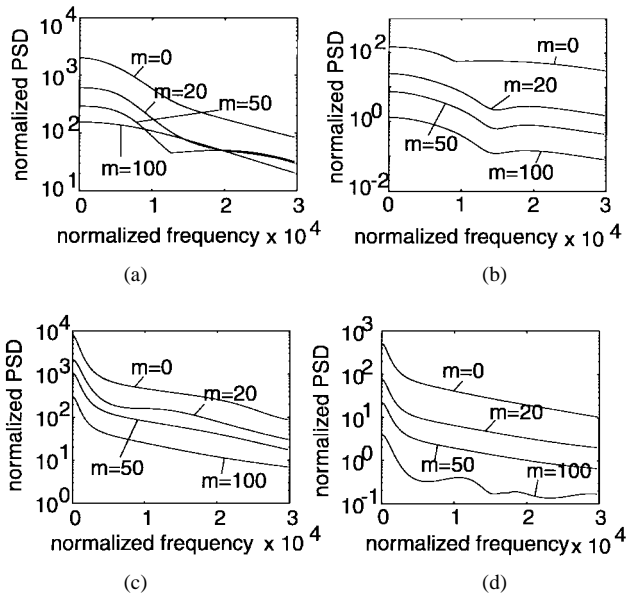


Fig. 6. Channel PSD with directional driving pattern. (a)  $E_b/N_0 = 20$  dB. (b)  $E_b/N_0 = 30$  dB, with random driving pattern. (c)  $E_b/N_0 = 20$  dB. (d)  $E_b/N_0 = 30$  dB.

turns right with  $P_r$  or goes straight on the same street with  $P_s$ . For the directional driving, we assume  $P_s = 0.6$ ,  $P_r = 0.2$ , and  $P_l = 0.2$ . For the random driving,  $P_s = P_r = P_l = 1/3$ .

In the power distribution, we consider two average SNR levels in each cell, defined by  $E_b/N_0 = 20$  dB and 30 dB. In the selection of channel coding schemes, we assume to use the Reed–Solomon code where the number of correctable bit errors in each packet  $m$  can be set at 0, 20, 50, or 100. Of course, the coding overhead increases with  $m$  [23]. We further fix the channel speed at 1.92 Mbit/s and the size of each packet at  $n = 480$  bits, which includes the  $2m + 1$  coding bits for error correction. Based on these conditions, one can use the original  $\text{SNR}(t)$  trace, collected in the downtown Austin area, to generate various  $R_c(t)$  traces and so to collect the statistics of  $R_c(t)$ . We use 14 h of  $R_c(t)$  sequence for simulation and analysis throughout the paper.

Fig. 6(a) and (b) shows the PSD of  $R_c(t)$  in the directional driving at  $m = 0, 20, 50$ , and 100, with respect to  $E_b/N_0 = 20$  dB in Fig. 6(a) and 30 dB in Fig. 6(b).<sup>1</sup> Clearly, increasing  $m$  has the effect of reducing channel PSD because of the improved packet success rate, but this is achieved at the expense of its much reduced number of user information bits in each packet, which is equivalent to the reduction of effective channel capacity. The inspection of Fig. 6(a) and (b) shows that increasing  $E_b/N_0$  also has the effect of reducing channel PSD at each given  $m$ , which is obvious due to the improved bit error rate performance within the cell. Note that while the average of  $R_c(t)$  increases with the increase of  $E_b/N_0$  or  $m$ , the variance and total power of  $R_c(t)$  decreases with the increase of  $E_b/N_0$  or  $m$ . Yet, increasing  $E_b/N_0$  in this cell will also cause the increase of its noise level in the neighborhood cells, which is not considered in our study.

<sup>1</sup>For the purpose of comparison between the service PSD and the arrival PSD in queueing analysis, both power spectra and their frequency need to be normalized by the average channel capacity. See [24] for details.

Similar performance is observed in Fig. 6(c) and (d) in the random driving. As compared to the directional driving in Fig. 6(a) and (b) the random driving reveals much increased LF energy at each given  $m$  and  $E_b/N_0$ . This is because in our particular example the random driving tends to stay longer in the vicinity of a certain area as compared the directional driving, thus increasing the autocorrelation of the signal attenuation over time. Note that such a power comparison can be changed with different driving patterns. For example, if we have  $P_s = 0.1$ ,  $P_r = 0.8$ , and  $P_l = 0.1$  for directional driving, which represent mostly turning right at each cross section, we will stay longer in the vicinity of a certain area compared to the above mentioned random driving pattern. Our main point here is that driving pattern can change the channel dynamics as well as queueing performance as we will soon observe.

One may find that the channel PSD has a significant amount of energy in its LF region, which is mainly contributed by the shadowing dynamics. The energy of multipath fading dynamics spreads out over a much larger frequency region.

#### D. Decomposed Channel Statistics

According to the work in [14], one can decompose the traffic dynamics into three frequency regions: LF region in  $0 < |\omega| \leq \omega_L$ , HF region in  $|\omega| \geq \omega_H$ , and MF region in  $\omega_L < |\omega| < \omega_H$ . The study in [14] further gives the engineering guideline  $(\omega_L, \omega_H) = (0.01\pi/d_{\max}, 2\pi/d_{\max})$  for the frequency division in measurement.  $d_{\max}$  is the maximum queueing delay in the fluid-flow queueing model, given by  $K/\mu$  where  $K$  is buffer capacity and  $\mu$  is the average service rate. The main result in [14] has the following practical implications. For the LF traffic, one only needs to measure the first-order statistics (CDF), especially the tail portion of its distribution. For the MF traffic, both first- and second-order statistics (CDF and PSD) are important to measure for queueing analysis. For the HF traffic, no statistics need to be measured since the buffer perfectly absorbs its dynamics. The extension from traffic dynamics to channel dynamics is straightforward.

By capturing the only important channel statistics, one can build a simple but accurate channel model for queueing analysis of wireless multimedia transmission over fading channel. For instance, if the channel PSD contains most energy in the LF region, we only need to build a channel model to match the CDF without loss of queueing solution accuracy. On the other hand, if the channel PSD contains most energy in the HF region, one can neglect the entire channel dynamics in modeling. Only when the channel contains significant amount of energy in the MF region, the channel model must be built to match both CDF and PSD.

#### E. Packet Arrival Statistics

As commonly observed in traffic measurement, most multimedia traffic streams have their energy highly concentrate on LF band, which is attributed to the long range dependence or large time-varying scale of packet arrivals. Fig. 7 shows such examples as collected from typical Ethernet data trace and JPEG video trace. One can use the techniques developed

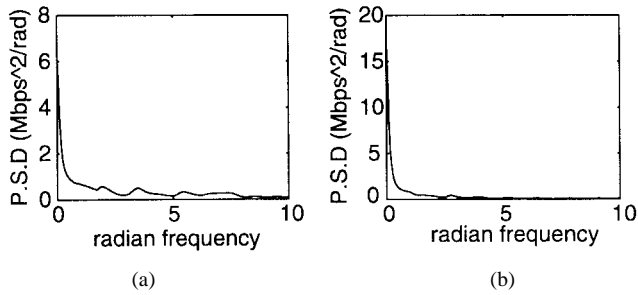


Fig. 7. Power spectrum of (a) Ethernet and (b) JPEG traces.

in [13] and [15] to build a Markov chain modulated process to match such statistics.

For simplicity, here we assume that the data arrival process consists of  $M$  independently, identically, distributed (i.i.d.) sources, each of which may represent a virtual connection on the channel. In this study we take  $M = 5$ . Each data source is modeled by a two-state Markov chain, defined by

$$\mathbf{Q} = \begin{bmatrix} -\beta & \beta \\ \alpha & -\alpha \end{bmatrix}, \quad \vec{\gamma} = [0, \gamma_{\text{on}}], \quad \pi = [1 - \epsilon, \epsilon]. \quad (12)$$

$\beta^{-1}$  and  $\alpha^{-1}$  are the average of the exponential ON- and OFF-periods,  $\gamma_{\text{on}}$  is the Poisson packet generation rate while in ON-period, and  $\epsilon = \beta/(\alpha + \beta)$  is the probability in ON-period. While  $\vec{\gamma}$  defines arrival rate in each state,  $\mathbf{Q}$  characterizes the time dynamics of the rate process.  $\vec{\pi}$  is the steady state probability distribution of the chain. One may associate each ON-period with a message generation time. The power spectrum of the aggregate sources can then be expressed by

$$P(\omega) = 2\pi\vec{\gamma}^2\delta(\omega) + \vec{\gamma} + \frac{B_1\sigma_\gamma^2}{(B_1/2)^2 + \omega^2} \quad (13)$$

with

$$\vec{\gamma} = M\epsilon\gamma_{\text{on}}, \quad B_1 = 2(\alpha + \beta), \quad \sigma_\gamma^2 = M\epsilon(1 - \epsilon)\gamma_{\text{on}}^2. \quad (14)$$

The impulse term in (13),  $2\pi\vec{\gamma}^2\delta(\omega)$ , represents the DC which is contributed by the nonzero average arrival rate  $\vec{\gamma}$ . The constant term,  $\vec{\gamma}$ , corresponds to the white noise effect of Poisson local dynamics in packet generation [12]. The last term in (13), which is our major interest, has the bell shape centered at zero frequency with its half power bandwidth given by  $B_1$  and the average power equal to the arrival rate variance  $\sigma_\gamma^2$ .

Three conditions are required for the two-state Markov chain design and to fix the arrival PSD. They can be taken from the source peak rate  $\gamma_{\text{on}}$ , source average rate  $\vec{\gamma}$ , and average message size  $\alpha^{-1}\gamma_{\text{on}}$ . Here we fix  $\gamma_{\text{on}}$  at  $\mu$  and  $\vec{\gamma}$  at  $\rho\{1 - E[\text{PER}(t)]\}\mu$  for each given  $\rho$ . In reality, the message size varies largely depending on applications. Increasing message size expands the correlation of packet arrivals, which is equivalent to increasing the LF power. Mathematically, increasing message size has the effect of reducing the bell bandwidth while keeping the average power unchanged. As a consequence, the arrival energy will concentrate more on the LF. We assume 500 packets per message on average in this paper.

### III. QUEUENIG RESPONSE

Here we investigate the queueing response to channel dynamics under various conditions, especially with respect to different driving patterns and fixed/adaptive channel coding schemes. To help us understand the role of channel PSD played in queueing performance, we first review the effect of multipath fading dynamics analyzed in [11]. In the study of queue response to shadowing and multipath fading dynamics, our focus will be on the identification of important channel statistics. A Markov chain modeling technique will then be presented to match such important channel statistics for network analysis.

#### A. Queueing Response to Multipath Fading

The study of the queueing response to multipath Rayleigh fading channel statistics in [11] reached two major conclusions. First, the channel PSD plays an important role in queueing analysis. Second, the queueing performance is strongly dependent on the interplay between arrival PSD and channel PSD, whichever has more LF energy will have stronger impact on the queueing solutions.

One of the most frequently used packet-level wireless channel model is a two-state Markov chain alternating between ON- and OFF-periods [8]. The average ON-period (OFF-period) is designed to match the average run length of consecutive packets which are successfully (unsuccessfully) transmitted. The statistical functions matchable by two-state Markov chains are rather limited. Its PSD function consists of a single bell component centered at the zero frequency; its CDF function only allows a single nonzero service rate in each ON-period. In contrast, one can use the SMAQ technique developed in [13] to built a multistate Markov chain to match both PSD and CDF functions in rather complicated forms, as done in [11]. Let us compare these two different channel modeling techniques in study of multipath fading channel dynamics for queueing analysis. Consider a multipath fading channel system, running at 2 Mbit/s rate with  $E_b/N_0 = 10$  dB and taking no error correction coding (i.e.,  $m = 0$ ).

The thick solid line in Fig. 8(a) shows the original channel PSD collected from an  $R_c(t)$  trace which is converted from the channel fading trace generated by the Jakes' method [25]. The same trace is used in computer simulation to obtain the original average queueing performance as a function of  $\rho$ , displayed in Fig. 8(b). The queue performance is measured in packet units.

The same channel fading trace is used to collect the average run lengths which are then applied to the construction of a two-state Markov chain model. The thin solid line in Fig. 8 shows the corresponding channel PSD and queueing solutions using the two-state Markov chain model. As compared to the original results, such a modeling can severely underestimate the LF energy of the channel, which is why the average queue length becomes significantly underestimated. For comparison purposes, we use the SMAQ tool to generate various Markov chain models to match the channel PSD in different degrees. Refer to the Appendix or [13] for the detail. For instance, one such Markov chain model has been designed to well match the LF channel PSD as shown in Fig. 8. Since the

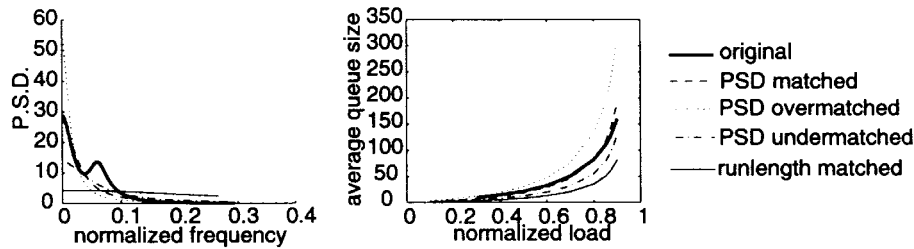


Fig. 8. Effect of PSD mismatching.

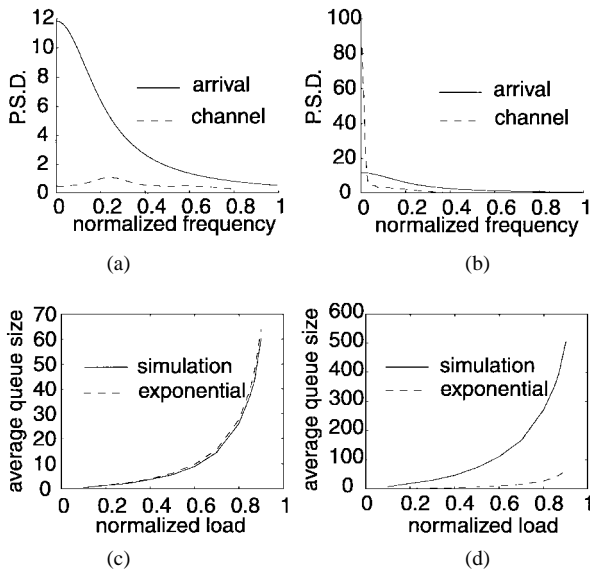


Fig. 9. Combination effect of channel PSD and arrival PSD. (a) 48 Kbit/s. (b) 8 Mbit/s. (c) 48 Kbit/s. (d) 8 Mbit/s.

queueing performance is mainly governed by the LF behavior of the channel, its average queue length is found in excellent agreement with the original one. For comparison purposes, we have constructed two additional Markov chain models. One of them undermatches the LF channel PSD while the other overmatches the LF channel PSD. As one can see in Fig. 8, the undermatched model leads to the queue length underestimation while the overmatched one leads to the queue length overestimation. Notice that all three Markov chain models, generated by the SMAQ tool, share the same average power and CDF. In other words, the first-order statistics of these three Markov models are identical. This example clearly indicates the importance of matching LF channel PSD in channel modeling to queueing performance analysis.

In the above example, we purposely designed the arrival PSD significantly less than the channel PSD, especially in the LF band. Hence, the queueing performance is mainly determined by the channel PSD. In general, the queueing performance should depend on the combination effect of the channel PSD and the arrival PSD in the low frequency band. To explore this idea, we consider two extreme cases. One case has a low-speed channel running at 48 Kbit/s; the other has a high-speed channel running at 8 Mbit/s. The rest of the channel conditions and the arrival statistics remain unchanged as in the above. The corresponding channel and arrival spectra of the two channels are plotted in Fig. 9(a) and (b). A high-

speed channel contains much more LF energy than a low-speed channel. The arrival PSD remains unchanged by the channel speed.

In the low-speed channel case, since the arrival PSD has much more LF energy than the channel PSD, the queueing performance should be mainly governed by the arrival PSD. In other words, one can completely ignore the channel spectral statistics in channel modeling and use a simple stochastic model like exponential server in queueing analysis. This is verified by the comparison of the queueing performance in Fig. 9(c) between the original channel trace and the exponential server model. In the high-speed channel case, the LF channel PSD can no longer be neglected by channel modeling. Otherwise, the queueing performance will be significantly underestimated as described in Fig. 9(d).

The study reveals the importance of comparing arrival PSD with channel PSD in the channel modeling. In principle, the channel dynamics need to be considered by channel modeling if and only if the LF channel PSD is comparable to the arrival PSD.

### B. Queueing Response to Shadowing and Multipath Fading

The shadowing and multipath fading dynamics contribute to the channel statistics in greatly different ways. The multipath fading is mainly caused by the motion of receiver and its variation is governed by the maximum Doppler frequency shift given by  $f_D = v/\lambda$  where  $v$  is mobile speed and  $\lambda$  is the wavelength [2]. In the scenario considered in the downtown Austin area, where mobile speed is less than 30 Km/h and carrier frequency is 1.9 GHz, the maximum Doppler frequency shift is in the range of around 50 Hz. In contrast, the shadowing occurs due to the irregular terrain and path loss. In a downtown area, the shadowing is mainly contributed by the buildings. The time scale of variation of shadowing is typically in the range of a few tens of second to a couple of minutes. In other words, much of the shadowing energy concentrate on a very LF band, typically less than 0.2 Hz.

Based on this inherent energy separation between the shadowing and multipath fading in the frequency domain, one can further compute the average multipath fading energy versus the average shadowing fading energy from the collected downtown Austin trace. For instance, the average multipath fading energy is found 1.3 times greater than the average shadowing energy under the condition  $(E_b/N_0, m) = (20 \text{ dB}, 0)$ , or 28 times greater under the condition  $(E_b/N_p, m) = (30 \text{ dB}, 100)$ . Although the multipath fading has much more energy than the shadowing, it is relatively evenly distributed over a much

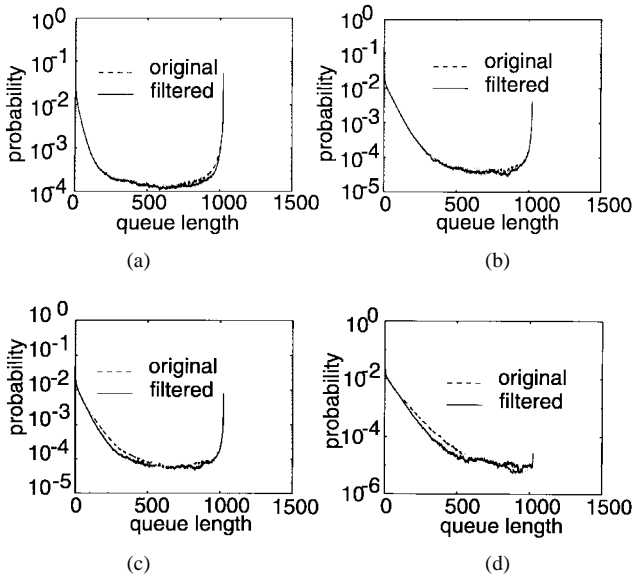


Fig. 10. Effect of multipath fading in the presence of shadowing given  $(E_b/N_0, m)$  equal to (a) (20 dB, 0), (b) (30 dB, 0), (c) (20 dB, 50), and (d) (30 dB, 50).

wider frequency range. In contrast, the highly concentrated energy distribution appeared in the LF band, as observed in Fig. 6, is solely attributed to the shadowing.

Similar to the effect of arrival PSD studied in [14], the queueing performance is expected to be much more affected by the LF channel dynamics (shadowing) as compared to the HF channel dynamics (multipath fading). This is because the HF variation of the channel service rate can be largely absorbed through the buffering system. To verify the dominance of shadowing dynamics in channel statistics, one can take the moving average operation to the original downtown Austin trace at every one second interval, such that the new filtered trace contains no multipath fading dynamics. Fig. 10 compares the simulation results of the queue distribution using both the original trace and the filtered trace given the buffer capacity  $K = 2^{10}$  and the system loading factor  $\rho = 0.9$ , over a wide range of selection of  $E_b/N_0$  and  $m$ . One can hardly observe queueing difference between the two traces. In other words, one can completely ignore the multipath fading dynamics in the presence of shadowing for queueing analysis.

### C. Queueing Performance to Various Factors

Given the assumption of the cell size of downtown Austin as in Fig. 2, here we examine the effect of driving patterns and buffer capacity on the queueing performance.

Let us replot Fig. 6(a) and (c) for the channel PSD of the directional and random drivings in Fig. 11(a) and (b) using the radian frequency unit. According to the frequency decomposition concept in Section II-C, the channel PSD can be further divided in LF, MF, and HF regions. The HF channel PSD has been largely ignored in Fig. 11(a) and (b) due to its negligible impact on the queue. The bound between the LF and MF regions is defined by  $\omega_L = 0.01\pi/d_{\max}$ .  $d_{\max}$  is the maximum allowable queueing delay which is dependent on the buffer capacity  $K$  and average channel service rate  $\mu$ . For

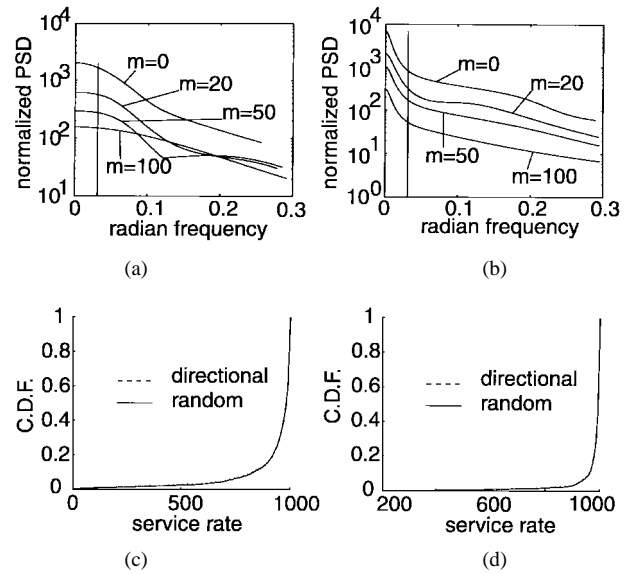


Fig. 11. Channel PSD with LF cutoff frequency. (a) Directional. (b) Random driving patterns and channel CDF with  $E_b/N_0 = 20$  dB. (c)  $m = 20$ . (d)  $m = 100$ .

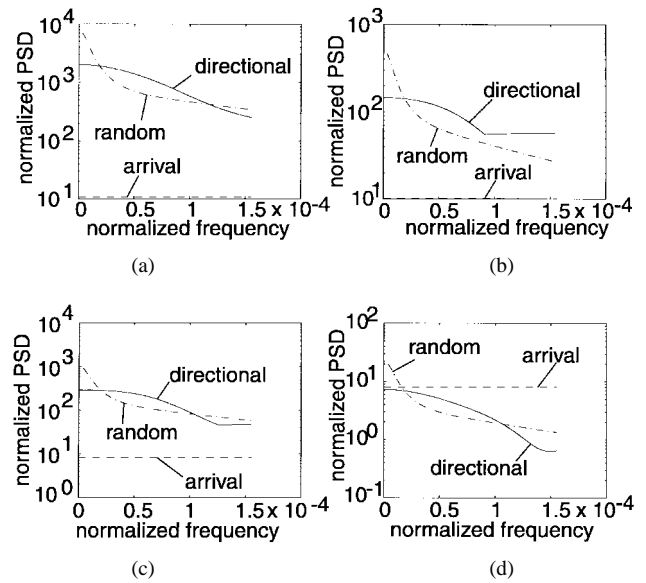


Fig. 12. Channel PSD versus Arrival PSD for  $(E_b/N_0, m)$  equal to (a) (20 dB, 0), (b) (30 dB, 0), (c) (20 dB, 50), and (d) (30 dB, 50).

$d_{\max} = K/\mu$ , we first take  $K = 2^{10}$  and  $\mu^{-1} = 1$  ms, such that  $d_{\max} = 1$  s as shown by the vertical line in Fig. 11(a) and (b) for the frequency division. One can find a significant amount of channel energy located in the LF region. Note that the channel CDF is independent of the driving patterns, which is further verified through the measurement of the real traces as compared in Fig. 11(c) and (d) at  $E_b/N_0 = 20$  dB for  $m = 20$  and 100.

In the queueing performance study, we consider four channel scenarios, represented by the pair of parameters  $(E_b/N_0, m)$  equal to (20 dB, 0), (30 dB, 0), (20 dB, 50) and (30 dB, 50), respectively. The channel PSD of the two driving patterns is further compared in Fig. 12 at each given scenario. Also plotted in Fig. 12 is the arrival PSD given the

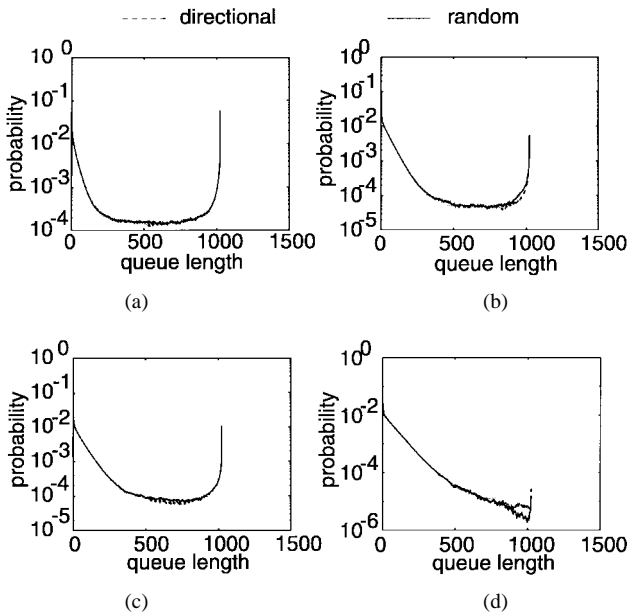


Fig. 13. Effect of driving patterns with  $K = 2^{10}$  for  $(E_b/N_0, m)$  equal to (a) (20 dB, 0), (b) (30 dB, 0), (c) (20 dB, 50), and (d) (30 dB, 50).

assumption of average 500 packets per message, which is negligible as compared to the channel PSD except in the last scenario. In Fig. 13, the queue distribution of the two driving patterns at  $\rho = 0.9$  are found in excellent agreement for all the scenarios. One may question why the queuing solutions are virtually identical given the significant difference in the channel PSD of the two driving patterns. This is because a large amount of channel energy is located in the LF region. Recall in Section II-C, the important channel statistics in the LF region are its CDF behavior, rather than the PSD behavior. Since the CDF behavior of the two driving patterns are basically identical, their queuing performance should not be significantly different. In other words, the channel modeling is sufficient to capture the CDF behavior in the LF region when the energy in the MF region is insignificant.

Such a modeling situation may change as the buffer capacity increases. For instance, let us increase the buffer capacity from  $K = 2^{10}$  to  $K = 2^{15}$ , which leads to the 32 times reduction of the boundary frequency  $\omega_L$  in Fig. 11(a) and (b). In consequence, much of the channel energy is now shifted from the LF region into the MF region, such that the MF energy becomes no longer negligible. This is why the difference in the queuing solutions of the two driving patterns now becomes significant as shown in Fig. 14, which is mainly caused by the difference of the two channel PSD's in the MF region. Especially since the directional driving always contributes less energy to the LF and MF regions as compared to the random driving, its queuing solutions also tend to be better than that of the random driving. For the last scenario in Fig. 14, the queuing difference between the two driving patterns is insignificant. This is because the arrival PSD, which is independent of the driving patterns, is no longer negligible as compared to the channel PSD.

Clearly, there are many system factors, such as the arrival PSD, buffer capacity, and driving pattern, which can greatly

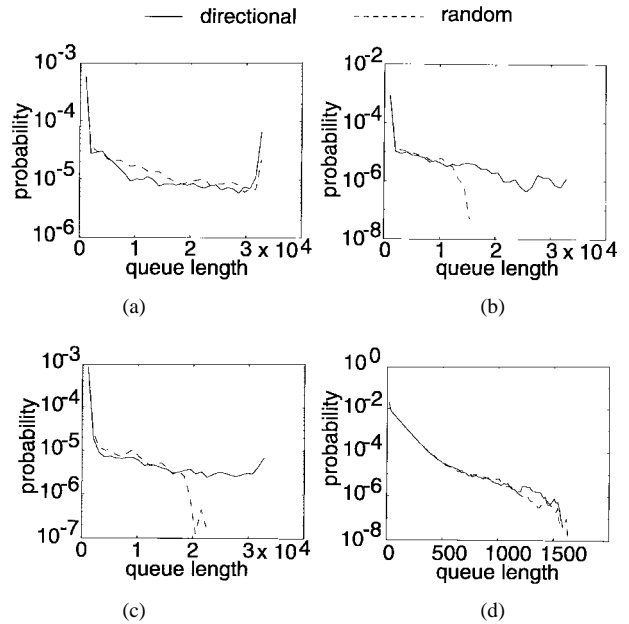


Fig. 14. Effect of driving patterns with  $K = 2^{15}$  for  $(E_b/N_0, m)$  equal to (a) (20 dB, 0), (b) (30 dB, 0), (c) (20 dB, 50), and (d) (30 dB, 50).

change the effect of channel statistics in each frequency region on the queuing performance.

#### D. Effect of Channel Coding

The LF channel dynamics (i.e., shadowing) are equivalently described by the large time scale variation behavior of the service rate. In other words, the more LF energy means the longer period of channel congestion once it occurs. One may adopt a proper error correction coding scheme to increase the success probability of each packet transmission, but this is achieved at certain expense of increased bandwidth overhead for coding. In fact, the bandwidth overhead for coding may even offset the bandwidth saving achieved by its increased packet success probability. In other words, the effective channel bandwidth and its associated queuing performance may even deteriorate when an excessive error correction coding scheme is adopted. Further, the coding theory is mainly developed using the traditional independent assumption of error occurrences in adjacent bits, whereas in reality they are highly correlated as described by the strong LF channel dynamics. Hence, the effectiveness of error correction coding in the shadowing wireless environment needs to be carefully examined.

The implementation of error correction coding can be either fixed or adaptive. While a fixed coding scheme is statically assigned and independent of the present channel condition, an adaptive coding scheme may dynamically select different coding schemes based on the observation of the present channel condition. The adaptive approach is expected to be particularly effective and practically feasible to cope with the slow time variation of the channel.

Consider the directional driving in a cell as in the previous study. Fix  $K = 2^{10}$  and  $\mu^{-1} = 1$  ms such that  $d_{\max} = 1$  s. Adopt the Reed–Solomon coding scheme at each given  $m$  except at  $m = 0$ . Fig. 15 shows the average queue

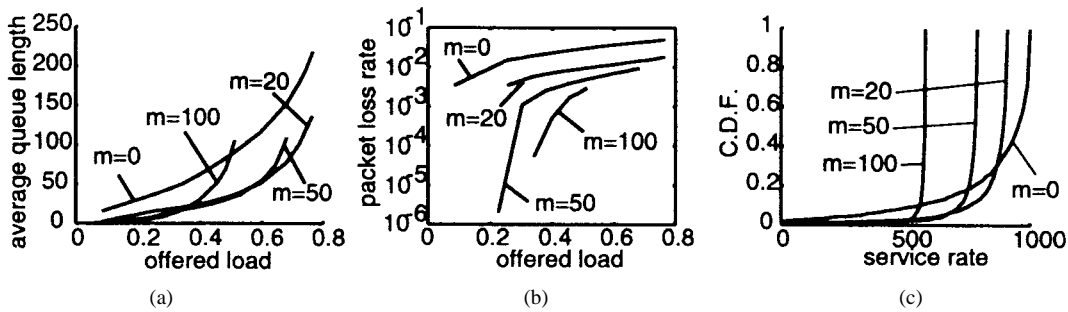


Fig. 15. Effect of fixed channel coding. (a) Queue length. (b) Packet loss rate. (c) CDF.

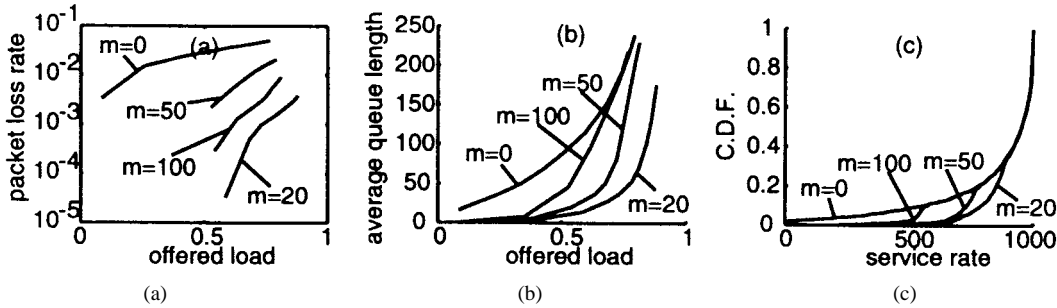


Fig. 16. Effect of adaptive channel coding. (a) Queue length. (b) Packet loss rate. (c) CDF improvement.

length and packet loss rate based on the downtown Austin trace for different  $m$  at  $E_b/N_0 = 20$  dB, using the fixed coding scheme. The offered load in Fig. 15, denoted by  $\rho$ , is defined by the ratio of the effective data arrival rate (i.e., excluding the channel coding overhead within each packet) to the total average channel capacity. Also plotted in Fig. 15(c) is the channel CDF performance. One can only achieve the maximum  $\rho < 50\%$  at  $m = 100$  subject to the average queue length of no more than 100 packets, versus 70% at  $m = 50$  under the same queue length constraint. The selection of  $m$  is dependent on the required packet queuing delay and loss rate performance for quality of services. For instance, if the service quality is mainly measured by the average queue length, one should choose  $m = 20$  to achieve the minimum queue length under the heavy load condition. On the other hand, if the service quality is mainly measured by the average loss rate subject to the loading condition  $\rho \leq 50\%$ , one may choose  $m = 100$  for the best loss performance. Note that the average loss rate can never be less than  $10^{-3}$  for  $\rho > 50\%$  by the fixed coding scheme, no matter which  $m$  is selected. In other words, while a fixed coding scheme can significantly improve the success probability of each packet in the channel congestion period, its overhead also reduces the effective transmission bandwidth in the channel noncongestion period.

This unbalanced issue can be overcome through either adaptive power control or adaptive channel coding. In our situation where the most deep fading occurs at the cell boundary, the adaptive channel coding is certainly more effective since the power increase at the cell boundary will increase the interference to other cells. Hence, we only consider the adaptive channel coding approach. For simplicity, we use a two-level adaptive coding scheme based on the detection of the present  $E_b/N_0$  level as compared to a given threshold  $SNR_{th}$ . If the present  $E_b/N_0$  is greater than  $SNR_{th}$ , i.e., in

the noncongestion period, no error correction coding will be implemented (i.e.,  $m = 0$ ). Otherwise, the Reed–Solomon coding scheme will be invoked with a preassigned  $m$ . The selection of  $SNR_{th}$  and  $m$  is dependent on the combination effect of the involved coding overhead versus the lost channel bandwidth without coding. That is, the coding will be invoked as soon as the lost channel bandwidth without coding exceeds the coding overhead. We assume an ideal situation where the present  $E_b/N_0$  value is made available to the mobile user and so the lost channel bandwidth without coding can be obtained from the corresponding packet loss rate. The coding overhead is also directly computable at each given  $m$ . The optimal  $SNR_{th}$  can then be identified.

In our case, we take  $m = 20, 50,$  and  $100$  for the adaptive coding. Fig. 16 provides the corresponding queue length and packet loss rate performance. For comparison purposes, the results without coding at  $m = 0$  is also displayed in Fig. 16. It is obvious that the adaptive coding achieves much better queueing/loss performance than no coding. Also plotted in Fig. 16(c) is the channel CDF performance. The inspection of Figs. 15 and 16 further show remarkable throughput/delay/loss performance improvement by the adaptive coding. This is mainly achieved by removing the unnecessary coding overhead in noncongestion periods. In general, the design of adaptive coding scheme is dependent on various system conditions, including channel statistics, arrival statistics, buffer capacity, and service quality requirement.

E. Measurement-Based Channel Modeling

So far our main focus has been on the identification of important channel statistics for queueing analysis, which is directly related to the interplay between channel PSD and arrival PSD in the LF region. Let us now concentrate on the Markov chain modeling of such channel statistics. It is

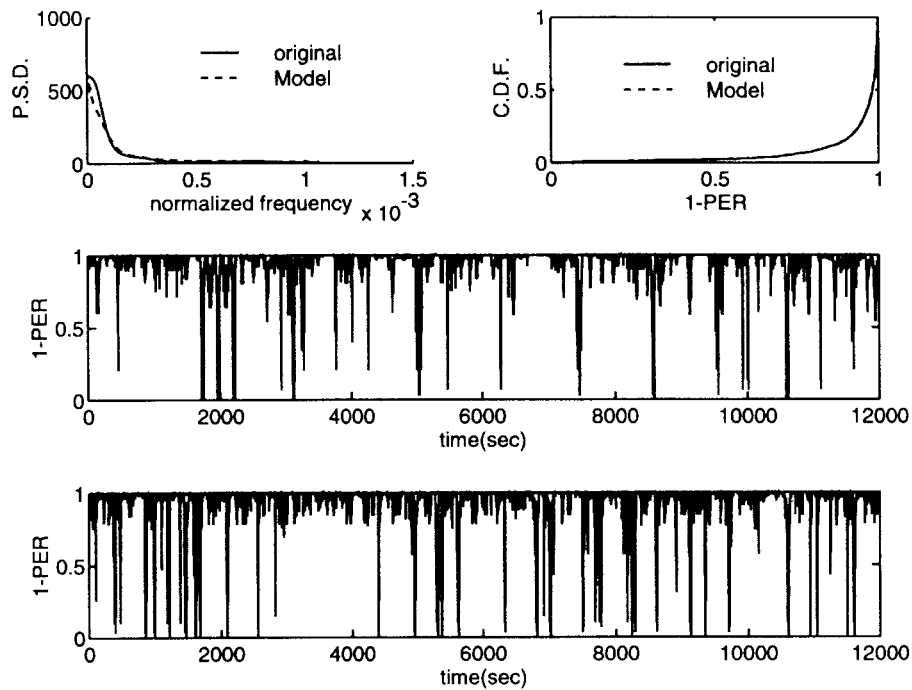


Fig. 17. Markov chain modeling of channel with fixed coding at  $m = 20$ .

obvious that the Markov chain channel modeling is necessary for queuing analysis if and only if the channel contains comparable LF energy to that of the arrival process. The SMAQ tool is used to build an MMP process, which can simultaneously match both CDF and PSD of the fading channel. Provided in the Appendix is the basic analytical framework of the SMAQ tool for such matching. One may refer to [13] and [15] for details. The SMAQ tool allows users to select a relatively large state space for Markov chain modeling, e.g., in the range of a few hundred states if necessary. A large state space is often chosen for the purpose of matching a long tail portion of CDF or a complex form of PSD structure. In fact, the Markov chain matching is one of the three basic components in SMAQ. The other two components are the statistic collection of any given traffic/channel trace and the analytical solution of the single finite-buffer queuing system constructed by the matched channel/traffic Markov chain models. The integration of the three components therefore provides us a unique solution technique for measurement-based queuing analysis [26], [27].

There are three basic guidelines for channel modeling, each of which applies to a different scenario of channel PSD versus arrival PSD. First, when arrival PSD is dominant over channel PSD, one can completely ignore the channel dynamics and simply use an exponential or constant service rate model for queuing analysis. Second, when channel PSD is comparable with arrival PSD and has most energy in LF region, our modeling only needs to match the channel CDF in LF region. Third, when channel PSD is comparable with arrival PSD and has significant energy in MF region, our channel modeling needs to match both CDF and PSD functions. These guidelines can be readily extended from [14].

Let us take the same downtown Austin trace with the directional driving at  $E_b/N_0 = 20$  dB and  $m = 20$ . Its original

packet-level PSD and CDF statistics are collected in Fig. 17(a) and (b). One can then use the SMAQ tool to build a 401-state Markov chain to match the two statistic functions as also shown in Fig. 17(a) and (b). Compared in Fig. 17(c) and (d) are one segment of the original PER trace versus a man-made PER trace generated by the matched Markov chain. As one can see, the two PER traces are statistically alike. Similar observations are made in Fig. 18 when the two-level adaptive coding scheme at  $m = 20$  is adopted.

We now compare the queuing solutions between using the original trace and using the Markov generated trace by computer simulation, under various conditions. In the first case, the channel is represented by  $E_b/N_0 = 20$  dB with the adaptive coding. The buffer capacity is fixed at  $K = 2^{10}$ . There are 500 packets per message on average for the data arrival statistics. Fig. 19(a) shows the corresponding channel PSD and arrival PSD, where the channel PSD is found to be dominant over the arrival PSD and have most energy in the LF region. According to the above mentioned guidelines, only the channel CDF in the LF region needs to be matched by the modeling, which is achieved using a 101-state Markov chain by the SMAQ tool. Fig. 19(b) shows the excellent agreement in the steady state queue distribution at  $\rho = 90\%$  between using the original trace and using the matched Markov chain model. In fact, the queue average and standard variation are all matched very well over a wide range of utilizations as found in Fig. 19(c) and (d).

The only change in the second case is to increase the buffer capacity from  $K = 2^{10}$  to  $K = 2^{13}$ , which is equivalent to the increase of  $d_{\max}$  by eight times. In consequence, a significant amount of energy has been shifted from the LF region into the MF region. Based on the guidelines, one can no longer neglect the channel statistics in the MF region. The SMAQ tool is used to generate a 401-state Markov chain to match both channel

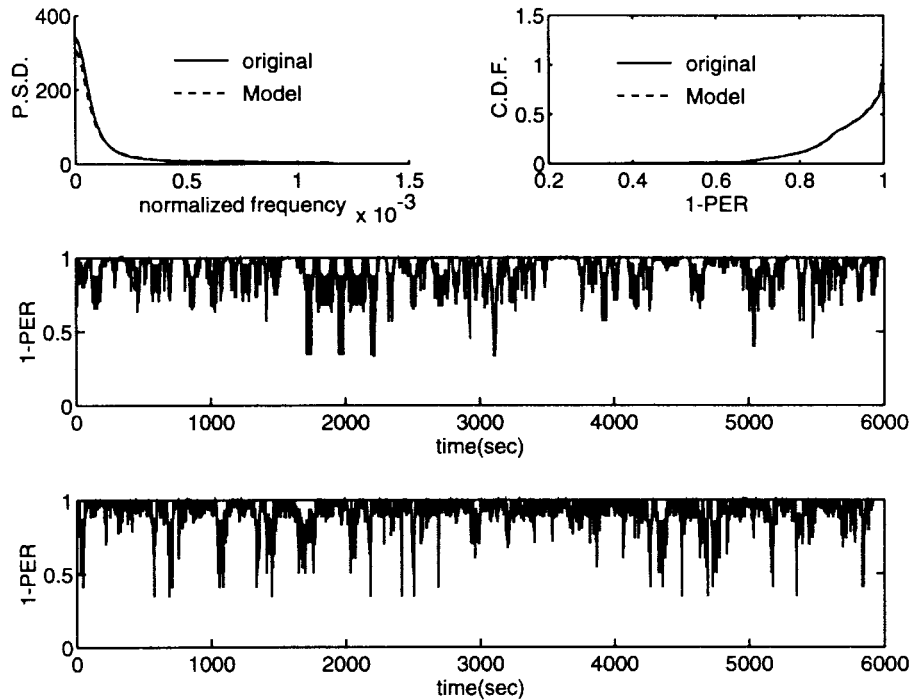


Fig. 18. Markov chain modeling of channel with adaptive coding at  $m = 20$ .

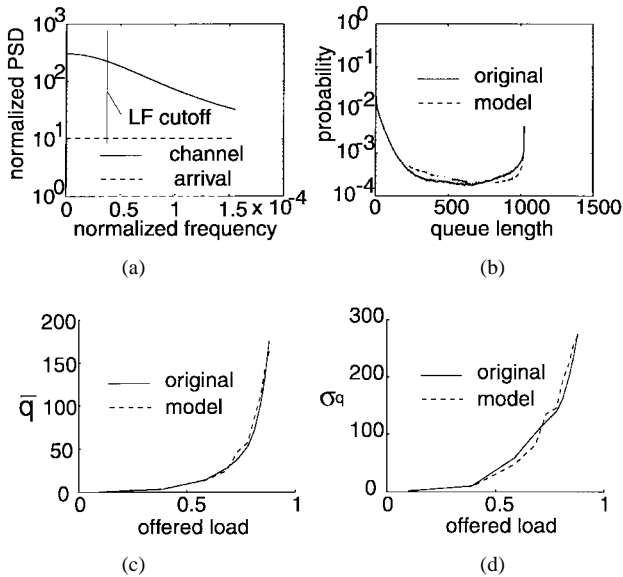


Fig. 19. Channel modeling with adaptive coding at  $m = 20$  with  $K = 2^{10}$ . (a) Arrival PSD versus channel PSD with LF cutoff frequency. (b) Queue distribution at  $\rho = 0.9$ . (c) Average queue length. (d) Queue standard deviation.

CDF and PSD functions, at  $m = 20$  with the adaptive coding. Again, the queueing solution comparison between the original trace and the Markov chain modeling in Fig. 20 shows an excellent agreement over a wide range of utilizations.

In the third case, we increase the signal strength from  $E_b/N_0 = 20$  dB to 30 dB and reinforce the adaptive coding at  $m = 100$  while still fix  $K$  at  $2^{10}$ . As a consequence, the channel PSD is much reduced. As shown in Fig. 21(a), the arrival PSD now becomes dominant over the channel PSD. From one of the guidelines, one can completely ignore the

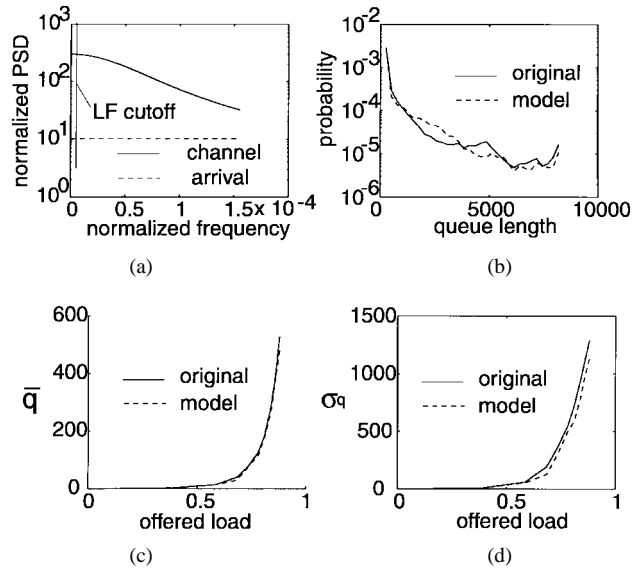


Fig. 20. Channel modeling with adaptive coding at  $m = 20$  with  $K = 2^{13}$ . (a) Arrival PSD versus channel PSD with LF cutoff frequency. (b) Queue distribution at  $\rho = 0.9$ . (c) Average queue length. (d) Queue standard deviation.

channel dynamics and simply use an exponential server as the channel model. This is confirmed by the matched queueing solutions in Fig. 21.

The measurement-based channel modeling technique developed here provides us a viable approach for high-layer wireless network analysis.

IV. CONCLUSION

In this paper, we have characterized the packet-level statistics of shadowing and multipath fading channel dynamics and

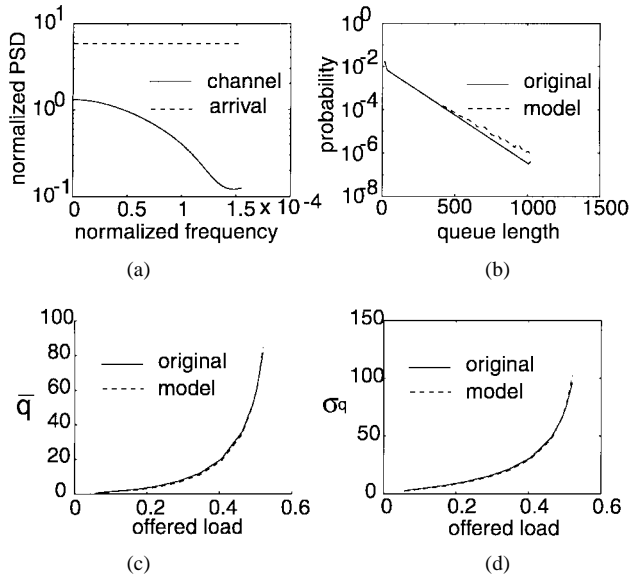


Fig. 21. Channel modeling with adaptive coding at  $m = 100$  with  $K = 2^{10}$ . (a) Arrival and channel PSD. (b) Queue distribution at  $\rho = 0.9$ . (c) Average queue length. (d) Standard deviation of queue length.

examined their impact on queueing performance under various conditions, such as different  $E_b/N_0$ 's, driving patterns, coding schemes, and buffer capacities. The measurement of channel statistics are decomposed into three different frequency regions, each of which has a significantly different impact on the queueing performance. Given the arrival statistics, channel statistics, and buffer capacity in a system, we developed the basic guidelines to capture the important channel statistics in channel modeling. In particular, the multipath fading statistics are found to be negligible as compared to the shadowing statistics for network performance study. Further, the adaptive error correction coding scheme is found to be highly effective to cope with the slow time variation of a shadowing channel for network performance improvement. Our channel statistics analysis gives a clear picture to the understanding of queueing performance in wireless network environment. The measurement-based channel modeling technique introduced in this paper further provides a new direction toward the integration of wireless channel modeling and network performance analysis. Future work include the extension of the present single channel modeling to the network modeling of multiple channels which are statistically shared by multiple users at geographically different locations.

#### APPENDIX

This appendix provides the background knowledge of Markov chain construction to match the first and second-order statistics of a rate process  $\gamma(t)$ , which in our case is the packet service rate process  $R_c(t)$  of a multipath fading channel.

Consider an  $N$ -state MMP defined by its transition rate matrix  $\mathbf{Q}$  and service rate vector  $\vec{\gamma} = [\gamma_0, \gamma_1, \dots, \gamma_{N-1}]$ , where  $\gamma_i$  is the service rate when the Markov chain is in state  $i$ . The autocorrelation function of the rate process is expressed by  $R(\tau) = \overline{\gamma(t)\gamma(t+\tau)}$ . The Markov chain constructed by

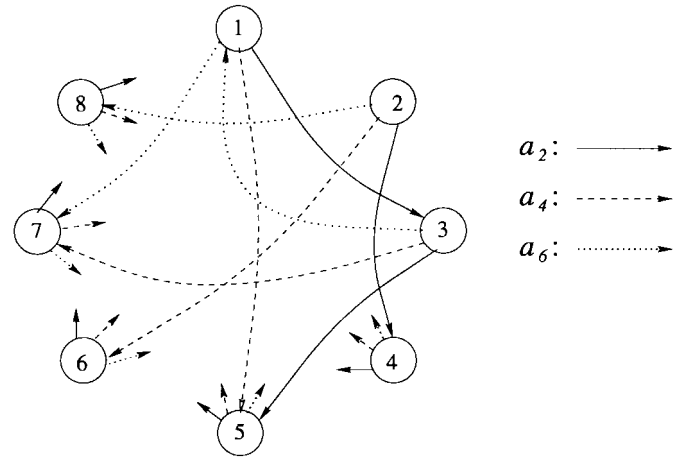


Fig. 22. An example of 8-state circulant with nonzero transition rates  $a_2$ ,  $a_4$ , and  $a_6$ .

the SMAQ tool must be of circulant type. That is, each row of  $\mathbf{Q}$  is a forward shift permutation of the previous row, denoted by  $\vec{a} = [a_0, a_1, \dots, a_{N-1}]$  with  $\mathbf{Q} = \text{circ}(\vec{a})$ . Fig. 22 shows an example of eight-state circulant. One important feature of such a circulant matrix is that all the eigenvalues of  $\text{circ}(\vec{a})$  are distinct and expressed in closed form

$$\vec{\lambda} = \sqrt{N} \vec{a} \mathbf{F}^* \quad \text{or} \quad \vec{a} = \frac{1}{\sqrt{N}} \vec{\lambda} \mathbf{F} \quad (15)$$

with  $\vec{\lambda} = [\lambda_0, \lambda_1, \dots, \lambda_{N-1}]$ , where  $\lambda_l$  is the  $l$ th eigenvalue of  $\mathbf{Q}$ .  $\mathbf{F}$  is a Fourier matrix with its  $(i, j)$ th element given by  $1/\sqrt{N} \exp[-(2\pi i j)/N] \sqrt{-1}$  and  $\mathbf{F}^{-1} = \mathbf{F}^*$ , where  $\mathbf{F}^*$  is the conjugate transpose of  $\mathbf{F}$ . For a stochastic matrix, we must get  $\lambda_0 = 0$ . Define a complex vector  $\vec{\beta} = [\beta_0, \beta_1, \dots, \beta_{N-1}]$ , which can be represented by two real vectors  $\vec{\psi} = [\psi_0, \psi_1, \dots, \psi_{N-1}]$  and  $\vec{\theta} = [\theta_0, \theta_1, \dots, \theta_{N-1}]$  with  $\psi_i = |\beta_i|^2$  and  $\theta_i = \arg\{\beta_i\}$  given  $-\pi < \theta_i \leq \pi, \forall i$ . That is,  $\theta_i$  is the principal value of the argument of  $\beta_i$ . We then have

$$\vec{\psi} = |\vec{\beta}|^2 = \frac{1}{N} |\vec{\gamma} \mathbf{F}^*|^2 \quad \text{or} \quad \vec{\gamma} = \sqrt{N} \vec{\beta} \mathbf{F}. \quad (16)$$

Its PSD is then expressed by

$$P(\omega) = 2\pi \vec{\gamma}^2 \delta(\omega) + \sum_{l=0}^{N-1} \psi_l b_l(\omega) \quad (17)$$

with

$$b_l(\omega) = \frac{-2\lambda_l}{\lambda_l^2 + \omega^2} \quad \text{and} \quad \frac{1}{2\pi} \int_{-\infty}^{+\infty} b_l(\omega) d\omega = 1.$$

The first component in (17),  $2\pi \vec{\gamma}^2 \delta(\omega)$ , represents  $dc$  term, which exists due to the positive average arrival rate. In (17), each nonzero eigenvalue contributes a bell-shaped component  $b_l(\omega)$  to PSD. Every such component is represented by a bell-shaped curve located at the center frequency  $\text{Im}\{\lambda_l\}$  with half power bandwidth  $-2\text{Re}\{\lambda_l\}$  and weighted by the average power  $\psi_l$ . Hence, the PSD of a circulant modulated process (CMP) is captured by  $\vec{\lambda}$  and  $\vec{\psi}$ , where  $\vec{\psi}$  is nonnegative real. From (15)  $\vec{\lambda}$  is uniquely determined by  $\vec{a}$ . Also  $\vec{\psi}$  is uniquely determined by  $\vec{\gamma}$ . One can therefore eliminate the

bell component of  $\lambda_i$  simply by setting  $\psi_i = 0$ . When  $\psi_i = 0$ , the eigenvalue  $\lambda_i \in \vec{\lambda}$  is called *noneffective* and otherwise *effective*.  $P(\omega)$  is generally expressed by the superposition of multiple bell components.

Since the steady-state probability of each state in circulant is equally likely, i.e.,  $\pi_i = 1/N, \forall i$ , the CDF of CMP, denoted by  $F(x) = \int_0^x f(y) dy$ , only depends on  $\vec{\gamma}$ .  $F(x)$  is a piecewise multistep function which jumps by  $1/N$  at each individual value of  $x \in \vec{\gamma}$  in ascending order, as expressed by

$$F(x) = \lim_{t \rightarrow \infty} \Pr(\gamma(t) \leq x) = \frac{n_x}{N} \quad (18)$$

where  $n_x$  represents the number of arrival rates in  $\vec{\gamma}$  less than or equal to  $x$ . A wide range of CDF functions can be matched through the design of  $\vec{\theta}$ , after fixing PSD by  $\vec{\lambda}$  and  $\vec{\psi}$ . The variance of CMP is equal to the average arrival power  $\sum_{i=1}^N \psi_i \lambda_i$ . Refer to [13] for the detail construction of CMP to match the PSD and CDF of a given random process.

## REFERENCES

- [1] D. Huo, "Simulating slow fading by means of one dimensional stochastic process," in *Proc. IEEE VTC'96*, pp. 620–622.
- [2] M. J. Gans, "A power-spectral theory of propagation in the mobile radio environment," *IEEE Trans. Veh. Technol.*, vol. 21, pp. 27–38, Feb. 1972.
- [3] R. H. Clarke, "A statistical theory of mobile-radio reception," *Bell Syst. Tech. J.*, vol. 47, pp. 957–1000, July–Aug. 1968.
- [4] J. I. Smith, "A computer generated multipath fading simulation for mobile radio," *Bell Syst. Tech. J.*, vol. 24, pp. 39–40, Aug. 1975.
- [5] B. D. Fritchman, "A binary channel characterization using partitioned Markov chains," *IEEE Trans. Inform. Theory*, vol. 13, pp. 221–227, Apr. 1967.
- [6] S. Tsai, "Markov characterization of the HF channel," *IEEE Trans. Commun. Technol.*, vol. 17, pp. 24–32, Feb. 1969.
- [7] H. S. Wang and N. Moayeri, "Finite-state Markov channel—A useful model for radio communication channels," *IEEE Trans. Veh. Technol.*, vol. 44, pp. 163–171, Nov. 1995.
- [8] M. Zorzi, R. R. Rao, and L. B. Milstein, "On the accuracy of a first-order Markov model for data transmission on fading channels," in *Proc. IEEE ICUPC'95*, pp. 211–215.
- [9] M. Zorzi and R. Rao, "The effect of correlated errors on the performance of TCP," *IEEE Commun. Lett.*, vol. 1, pp. 127–129, Oct. 1997.
- [10] ———, "On the statistics of block errors in bursty channels," *IEEE Trans. Commun.*, vol. 45, pp. 660–667, June 1997.
- [11] Y. Y. Kim and S. Q. Li, "Modeling fast fading channel dynamics for packet data transmission," in *Proc. IEEE Infocom'98 Conf.*
- [12] S. Q. Li and C. L. Hwang, "Queue response to input correlation functions: Continuous spectral analysis," *IEEE/ACM Trans. Networking*, vol. 1, pp. 678–692, Dec. 1993.
- [13] ———, "On the convergence of traffic measurement and queueing analysis: A statistical-match queueing (SMAQ) tool," *IEEE/ACM Trans. Networking*, pp. 95–110, Feb. 1997.
- [14] Y. H. Kim and S. Q. Li, "Timescale of interest in traffic measurement for link bandwidth allocation design," *Proc. IEEE Infocom'96*, pp. 738–748.
- [15] H. Che and S. Q. Li, "Fast algorithms for measurement-based traffic modeling," *Proc. IEEE Infocom'97*, pp. 53–65; *IEEE J. Select. Areas Commun.*, to be published.
- [16] S. Q. Li, S. Chong, and C. Hwang, "Link capacity allocation and network control by filtered input rate in high speed networks," *IEEE/ACM Trans. Networking*, vol. 3, Feb. 1995, pp. 10–25.
- [17] S. Q. Li and J. D. Pruneski, "The linearity of low frequency traffic flow: An intrinsic I/O property in queueing system," *IEEE/ACM Trans. Networking*, vol. 5, pp. 429–443, July 1997.

- [18] W. C. Lau and S. Q. Li, "Traffic distortion and inter-source cross-correlation in high-speed integrated networks," *J. Comput. Telecommun. Networking*, vol. 29, pp. 811–830, Aug. 1997.
- [19] J. Ye and S. Q. Li, "Folding algorithm: A computational method for finite QBD process with level-dependent transitions," *IEEE Trans. Commun.*, vol. 42, pp. 625–639, Feb. 1994.
- [20] W. C. Y. Lee, *Mobile Communications Design Fundamentals*. New York: Wiley, 1993.
- [21] H. Ling, "Wireless channel modeling," [Online]. Available WWW: <http://ling0.ece.utexas.edu/comm/comms.html>, 1997.
- [22] B. Sklar, *Digital Communications Fundamentals & Applications*. Englewood Cliffs, NJ: Prentice-Hall, 1988.
- [23] S. Lin and D. J. Costello, *Error Control Coding: Fundamentals and Applications*. Englewood Cliffs, NJ: Prentice Hall, 1983.
- [24] H. D. Sheng and S. Q. Li, "Spectral analysis of packet loss rate at a statistical multiplexer for multimedia services," *IEEE/ACM Trans. Networking*, vol. 2, pp. 53–65, Feb. 1994.
- [25] W. C. Jakes, Jr., Ed., *Microwave Mobile Communication*. New York: Wiley, 1974.
- [26] S. Q. Li, S. Park, and D. Arifler, "SMAQ: A measurement-based tool for traffic modeling and queueing analysis, Part I—Design methodologies and software architecture," *IEEE Commun. Mag.*, vol. 36, pp. 56–65, Aug. 1998.
- [27] ———, "SMAQ: A measurement-based tool for traffic modeling and queueing analysis, Part II—Network applications," *IEEE Commun. Mag.*, vol. 36, pp. 66–77, Aug. 1998.



**Young Yong Kim** was born in Pusan, Korea, on May 12, 1968. He received the B.S. and M.S. degrees from the Seoul National University, Seoul, Korea, in 1991 and 1993, respectively. He is pursuing the Ph.D. degree in the Department of Electrical and Computer Engineering at University of Texas, Austin.

Since November 1998, he has been with the Wireless Network Management Research Group at Telcordia Technologies (formerly Bell Communication Research), Red Bank, NJ, as a Research Scientist. His interests include wireless channel modeling, performance evaluation of mobile networks, and design and analysis of the multimedia CDMA system.



**San-qi Li** (M'86) received the B.S. degree from the Beijing University of Posts and Telecommunications, Beijing, China, in 1976, and the M.A.Sc. and Ph.D. degrees from the University of Waterloo, Waterloo, Ont., Canada, in 1982 and 1985, respectively, all in electrical engineering.

From 1985 to 1989, he was Associate Research Scientist and Principal Investigator at Center for Telecommunication Research at Columbia University, New York. In September 1989, he joined the faculty of the Department of Electrical and Computer Engineering, University of Texas Austin, where he is presently Associate Professor. He has published more than 100 papers in international archival journals and refereed international conference proceedings. The main focus of his research has been developing new analytical methodologies and carrying out performance analysis of multimedia service networks, and based on these methodologies, understanding system fundamentals and exploring new design concepts. He is an Honorable Professor at Beijing University of Posts and Telecommunication, China.

Dr. Li has served as a member of the Technical Program Committee for the IEEE INFOCOM Conference from 1988 to 1997. Since 1995, he has served as an Editor of IEEE/ACM TRANSACTIONS ON NETWORKING.